

Giant Zero-Bias Conductance and Multiple Andreev Reflections in Carbon Nanotubes with Superconducting Contacts.

A. Makarovski,¹ J. Liu,² and G. Finkelstein¹

¹ *Department of Physics, Duke University, Durham, NC 27708 and*

² *Department of Chemistry, Duke University, Durham, NC 27708*

Superconducting metal leads strongly modify the electronic conductance through carbon nanotubes. Depending on the nanotube transparency, which is controlled by the gate voltage, we observe a strong enhancement of the zero-bias conductance (way above the ballistic limit of $4e^2/h$) or formation of a tunneling gap. Subgap structures corresponding to the Multiple Andreev Reflections are also found. At intermediate transparencies, the zero-bias differential conductance demonstrates unexpected non-monotonic temperature dependence.

PACS numbers: PACS numbers: 73.63.Fg, 73.23.Hk, 74.45.+c, 74.50.+r

INTRODUCTION

Carbon nanotubes exhibit a variety of interesting transport phenomena at low temperatures [1]. A number of studies addressed the behavior of nanotubes attached to superconducting leads [2–8]. The initial studies concentrated on suspended nanotubes and nanotube bundles [2, 3], gated proximity effect in nanotubes [4], and multi-wall nanotube Quantum Dots with superconducting leads [5, 6], while the recent measurements demonstrated a gated supercurrent through a single wall nanotube [7].

In this work, we investigate transport through nanotubes contacted by superconducting Pb leads. We find that the nanotube differential conductance $G \equiv dI/dV$ at small bias may be enhanced or suppressed depending on the transparency of the nanotube, which serves as a weak link between the two bulk superconductors. In particular, at high nanotube transparencies (measured when superconductivity in the leads is suppressed) we find a strong enhancement of zero-bias conductance, up to $10e^2/h$ in some of our samples. This value greatly exceeds the ballistic limit of $4e^2/h$ achievable in single-wall nanotubes with normal metal leads. We can control the nanotube transparency by changing the gate voltage, and observe that at small transparencies, the zero bias conductance is suppressed, and prominent subgap features appear at finite source-drain bias V_{SD} . Finally, at intermediate transparencies, we observe a non-monotonic temperature dependence of the zero-bias conductance peak, which goes through a maximum as the temperature is lowered.

The carbon nanotubes were grown by a CVD method using CO as a feedstock gas [9] on top of a degenerately doped Si/SiO_2 substrate, which serves as a gate. The average diameter of nanotubes in this sample is 2–3 nanometers, indicating that most of the nanotubes are single or double walled. Metal electrodes to the nanotubes were patterned by e-beam lithography. We choose to use Pb as the electrode material for its rel-

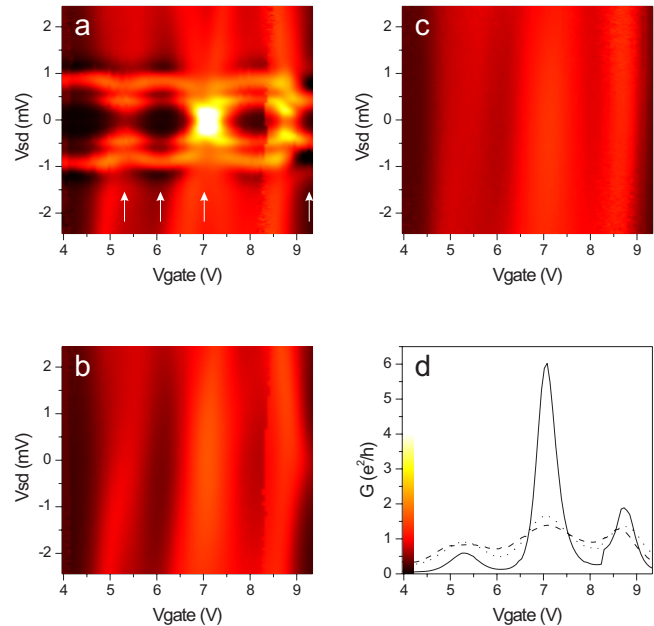


FIG. 1: Differential conductance of a 100 nm-long nanotube as a function of the gate voltage V_{gate} (horizontal axis) and the source-drain bias V_{SD} (vertical axis) at a) $T = 1.2$ K, $B = 0$; b) $T = 1.2$ K, $B = 0.5$ T; and c) $T = 10$ K, $B = 0$. In b) and c) superconductivity in the leads is suppressed. In a) superconductivity in the leads induces greatly enhanced conductance ($V_{gate} \approx 7.1$ V, $V_{SD} \approx 0$), the gap and the subgap features at $V_{SD} \sim \pm 1$ mV and ± 0.5 mV. d) Differential conductance as a function of V_g at $V_{SD} = 0$ corresponding to Figures 1a-c. Solid line: case a); dotted line: case b); dashed line: case c). Colored bar: the color map of Figures 1a-c going from 0 to $4e^2/h$.

atively high transition temperature of 7.2 K. Since Pb itself was found to form low transparency contacts to the nanotubes, a 15 nm Pd/Au alloy contact layer was deposited directly on the nanotube, immediately followed by the 70 nm Pb layer. While the nanotube is not contacted by Pb directly, we expect the proximity-induced superconductivity permeate through the thin

Pd/Au film. Indeed, recent STM measurements demonstrated proximity-induced superconducting gap in gold films of a comparable or larger thickness deposited on top of Nb substrate [10]. We have checked that the leads become normal at $T \sim 7$ K and zero magnetic field. At the lowest temperature of 1.2 K we find that superconductivity in the leads may be suppressed by a perpendicular magnetic field of ~ 0.4 T. We use both the temperature and magnetic field to tune the superconducting properties of the electrodes. We measure the differential conductance of the sample $G(V_{SD}, V_{gate})$ by a standard AC technique at the excitation level of 10-50 μ V RMS (voltage-biased).

SHORT NANOTUBES

Figures 1a-c show the differential conductance of a 100 nm - long nanotube (sample A) presented as a color map as a function of the source-drain bias V_{SD} and the gate voltage V_{gate} at three different magnetic fields and temperatures: a) $T = 1.2$ K, $B = 0$; b) $T = 1.2$ K, $B = 0.5$ T; and c) $T = 10$ K, $B = 0$. The magnetic field of 0.5 T directed perpendicular to the nanotube or the temperature of 10 K are not expected to noticeably change the nanotube transparency, while the superconductivity in the leads is suppressed. (Perpendicular magnetic field introduces only Zeeman, not orbital splitting of the nanotube energy levels; 0.5 T corresponds to the Zeeman splitting of ~ 0.5 K.) Therefore, we view Figures 1b and 1c as the transparency maps of the nanotube with normal leads.

In Figure 1d we show the zero-bias conductance measured at the same three sets of parameters as in Figures 1a-c (the line graphs in Figure 1d could be viewed as horizontal cross sections of Figures 1a-c). We see that as the superconductivity in the leads is suppressed, either by application of magnetic field or at elevated temperature, the nanotube conductance demonstrates very broad oscillations in V_{gate} . We associate these oscillations with the single-particle interference of electronic waves reflected from the metal contacts [11]. One of the tunneling barriers that couples this nanotube to the leads is evidently more transparent than the other. Indeed, we notice that the widths of the peaks in the normal state conductance in Figure 1d are comparable to their separations. Therefore, at least one of the barriers has to be very transparent. Its presence suppresses the charging effects in the nanotube. The conductance is limited below $1.5e^2/h$ by the second, more opaque barrier. The more transparent barrier results in the life-time broadening Γ comparable to the level spacing Δ ($\Delta \gtrsim 10$ meV, as confirmed by measurements at higher V_{SD}). We also see, looking at the Figures 1b and c, that the data is featureless in the V_{SD} (vertical) direction. Thus for a given gate voltage, the nanotube transparency does not depend on energy on the scale of $\gtrsim \Delta/e$. Therefore, we may consider the

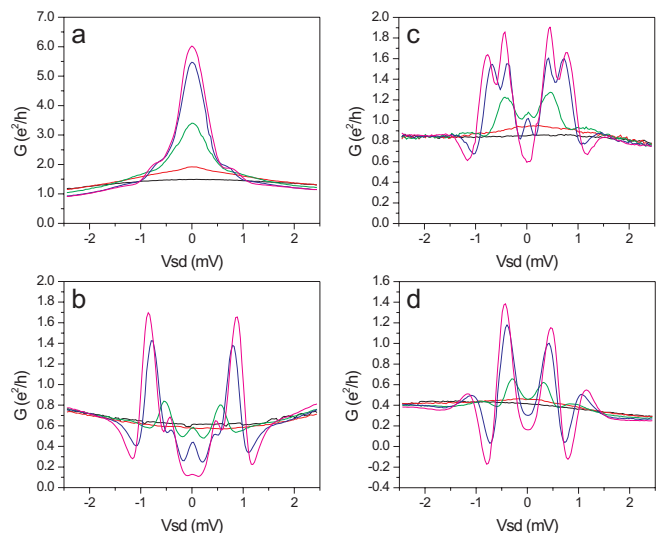


FIG. 2: Conductance measured vs. V_{SD} at four gate voltages for the same sample as in Figure 1 at different temperatures: 7.5 K (black), 5.5 K (red), 4.0 K (green), 2.5 K (blue), 1.2 K (purple). a) $V_{gate} = 7.1$ V, maximal nanotube transmission. Zero-bias conductance increases at low temperatures way above the ballistic limit of $4e^2/h$ possible for normal contacts. b) $V_{gate} = 6.1$ V, local minimum of the nanotube transmission. Zero-bias conductance decreases as the temperature is lowered and the 2Δ features are prominent at $V_{SD} \approx \pm 0.8$ mV. c) $V_{gate} = 5.3$ V, intermediate nanotube transmission. As the temperature is decreased, the zero-bias peak first grows, but then vanishes. Subgap features are clearly visible at $V_{SD} \approx \pm 0.4$ mV. d) $V_{gate} = 9.3$ V. Negative differential conductance is observed at $V_{SD} \approx \pm 0.8$ mV.

whole nanotube as a single tunneling barrier with gate-controlled transparency.

When the leads become superconducting in Figure 1a, several features become visible: *i*) a region of enhanced conductance at $V_{SD} \approx 0$ and $V_{gate} \approx 7.1$ V; *ii*) horizontal features at $V_{SD} \sim \pm 1$ mV and $\sim \pm 0.5$ mV; *iii*) regions of suppressed conductance at $V_{SD} \sim 0$ and extended ranges of V_{gate} . These features correspond to: *i*) enhanced conductance between two superconducting leads due to the establishment of a weak link through the nanotube; *ii*) Multiple Andreev Reflection features (**MAR**) at resonant energies of $2\Delta/n$, where n is an integer [12–15]; *iii*) tunneling gap between two weakly coupled superconducting leads. In the following we consider these features in detail.

Figure 2 shows the nanotube differential conductance measured as a function of V_{SD} for several temperatures at $B=0$ T and at several values of the gate voltage. Each of the curves in Figures 2a-d can be viewed as a vertical slice through a map similar to Figures 1a,c at a fixed gate voltage (the corresponding gate voltages are indicated by arrows in Figure 1a). At all gate voltages, the highest temperature data ($T = 7$ K) demonstrates only minor

variations with the source-drain bias. This stresses our notion that the nanotubes form a weak link with energy-independent transmission. The behavior of conductance as a function of magnetic field is very similar, and these data will be omitted for brevity.

In Figure 2a, we consider nanotube conductance at the gate voltage $V_g = 7.1$ V corresponding to the maximum of the differential conductance. The nanotube conductance is relatively insensitive to the temperature changes in the range $T > 7$ K. As the leads become superconducting at lower temperatures, a peak grows at small V_{SD} (Figure 2a). The peak greatly exceeds the ballistic limit of conductance ($4e^2/h$) possible for a complete transmission of the four modes in the nanotube with normal leads. Similar peak in dI/dV was observed in [5, 6, 8] and indicates the establishment of a weak link between the two superconducting leads. In principle, one may expect to observe signatures of a supercurrent (which would correspond to an infinite dI/dV), similar to Ref. [7]. It was suggested that the inelastic scattering limits the zero-bias conductance [15, 16]. In this case, the height of the zero-bias peak in Figure 2a reflects the corresponding scattering time. The dependence of zero-bias conductance on temperature is shown by square symbols in Figure 5a. In this case the growth of the conductance saturates or even slightly decreases at $T \sim 2$ K. While we cannot exclude the possible spurious effects of the external electromagnetic environment, we note that in a more transparent sample the zero bias conductance does not saturate and continues to grow down to the lowest measured temperature (Figure 5b).

In Figure 2b, we show the temperature dependence of the nanotube conductance measured vs. V_{SD} at $V_{gate} = 6.1$ V corresponding to the low conductance region (arrow in Figure 1a). As the temperature or magnetic field is reduced, the zero-bias conductance drops, and the conductance peaks appear symmetrically at positive and negative V_{SD} . We attribute these features to the quasiparticle tunneling across the gap [12–15]. The superconducting gap in Pb is known to be $\Delta = 1.3$ meV. The significant (more than twofold) reduction of the gap in our measurements is likely caused by the proximity Au/Pd layer, which directly contacts the nanotube. A significant reduction of the gap has been measured in other nanotubes with composite superconducting contacts [5–8].

Going back to Figure 2a, we note that features at energies $\sim \pm 1$ meV are also visible there. The 2Δ and Δ peaks are expected to be washed away at high transparency (*cf.* Fig. 2 in [14] or Fig. 2 in [15]). The appearance of these features together with the high zero-bias peak indicates that more than one conductance mode is present. The more transparent mode is responsible for the zero-bias peak and the smooth background, while the less transparent mode adds the faint gap features. Indeed, in a single-wall Carbon nanotube two conductance

modes should exist, which become non-degenerate in the presence of mode-mixing scattering.

Another noticeable feature of the differential conductance in Figure 2b is a small peak formed at zero V_{gate} at intermediate temperatures, which is suppressed as the temperature is lowered. The peak is due to the enhanced density of states for the tunneling of the thermally excited quasi-particles at small biases, which is an effect that can be described within the single-particle "semiconductor model" [17]). As the temperature is reduced the thermal population of the quasi-particles decreases and the peak vanishes (Figure 5a, circles).

Figure 2c focuses on the region of intermediate transparency, where the subgap structures are best visible ($V_{gate} = 5.3$ V). In addition to the features at $\approx \pm 0.8$ mV, we see prominent peaks at $\approx \pm 0.4$ meV, which we identify with the MAR. The zero bias peak is again visible in Figure 2c. Here, the zero-bias conductance demonstrates a *non-monotonic* dependence on temperature (diamonds in Figure 5a).

Finally, Figure 2d demonstrates pronounced negative differential conductance (NDC) observed at $V_{gate} = 9.3$ V. The conductance deeps occur at the same $V_{SD} \approx \pm 0.8$ mV as the conductance peaks in Figures 2b and c. At the same time, the positions of the conductance peaks at $V_{SD} \approx \pm 0.4$ mV in Figure 2d coincide with the $\pm\Delta$ features in Figure 2c. The models of Andreev transport through a resonant level indeed predicted NDC [18, 19], however, it remains unclear why the conductance peaks at $V_{SD} \sim \pm 2\Delta/e$ turn into deeps, while the peaks at $V_{SD} \sim \pm\Delta/e$ survive.

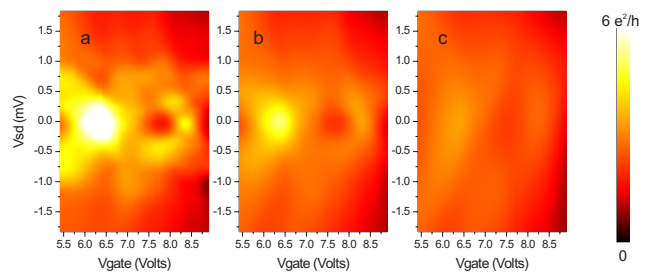


FIG. 3: Differential conductance maps as a function of V_{gate} and V_{SD} measured in 100 nm-long sample B at a) $B = 0$ T, b) $B = 0.2$ T and c) $B = 0.4$ T. Colormap: 0 to $6 e^2/h$.

Figure 3 shows the conductance maps as a function of V_{gate} and V_{SD} measured on another 100 nm-long nanotube (Sample B) at several values of the perpendicular magnetic field. As in Figure 1, the zero-bias conductance at some gate voltages is enhanced beyond $4e^2/h$ at low temperature and zero magnetic field. Application of magnetic field suppresses this enhanced conductance, but increases conductance elsewhere. This can be best seen in Figure 4a, where zero-bias conductance is shown as

a function of magnetic field. The zero-bias conductance in the absence of superconductivity (0.4 T) is greater than $2e^2/h$ in the whole range of gate voltages, and the Coulomb blockade is suppressed. The single-particle Fabry-Perot conductance oscillations are clearly visible. The arrows in Figure 4a indicate the gate voltages at which the V_{SD} dependence is recorded at several magnetic fields (Figures 4b-d). In Figures 4b and d, the conductance demonstrates a zero-bias peak exceeding $4e^2/h$ and MAR features, rather similar to Figure 2a. At the same time, in Figure 4c we see the development of the zero-bias dip, like in Figures 2b and 2c.

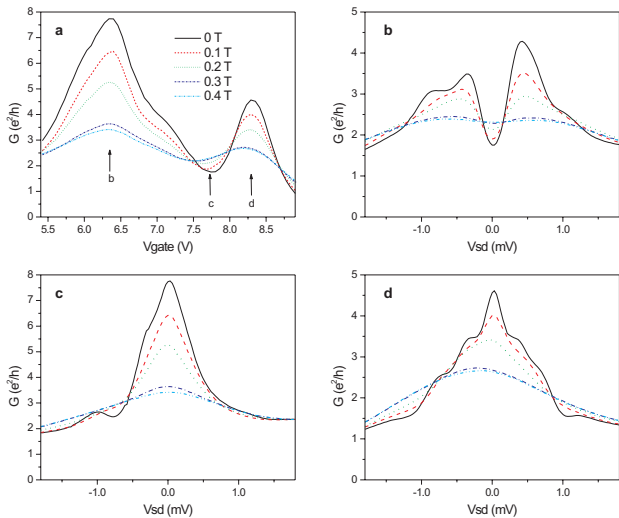


FIG. 4: a) Differential conductance of sample B as a function of V_{gate} at small bias. b-d) Differential conductance as a function of V_{SD} measured at $V_{gate}=6.3$ V, 7.7 V, and 8.3 V, respectively. (These gate voltages are indicated in Figure 4a by arrows.)

We summarize the temperature dependence of the zero-bias conductance at several gate voltages for the two 100 nm-long samples A and B in Figure 5. As discussed above, depending on the sample transparency, the conductance may *i*) grow as the temperature is lowered, *ii*) drop due to the suppression of the quasiparticle tunneling, or *iii*) demonstrate a non-monotonic behavior (more clearly seen in sample B, Figure 5b). We tentatively attribute this behavior to competition between the conductance enhancement followed by saturation (as in Figure 2a) and the suppression of the quasi-particle tunneling as the temperature is lowered (as in Figure 2b). A unified description of this behavior remains a challenge.

We now discuss the excess current I_{ex} , which unlike the zero-bias conductance should be relatively insensitive to the presence of inelastic processes. The excess current measured in sample A as a function of the normal state conductance is plotted in Figure 6. We use the value of $\Delta \approx 0.43$ meV extracted from the positions of the

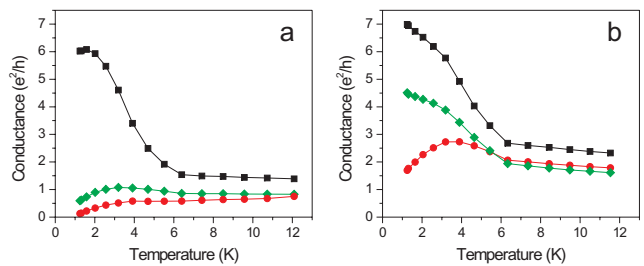


FIG. 5: Zero-bias conductance measured in the two 100 nm-long samples A and B as a function of temperature at several different gate voltages. Figure 5a corresponds to the same data as Figure 2. Squares: $V_{gate} = 7.1$ V (same as Figure 2a), circles $V_{gate} = 6.1$ V (same as Figure 2b), diamonds $V_{gate} = 5.3$ V (same as Figure 2c). Figure 5a corresponds to the same sample B as in Figures 3-4. Squares: $V_{gate} = 6.3$ V, circles: $V_{gate} = 7.7$ V, diamonds: $V_{gate} = 8.3$ V.

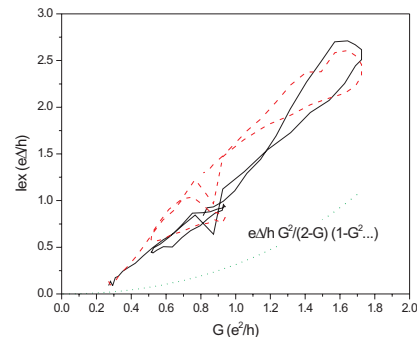


FIG. 6: Excess current measured at $V_{SD} = \pm 1.8$ mV in sample A (solid and dashed lines). The data are extracted from Figures 1a and 1b in the range of $V_{gate} = 4-8$ V. Dashed line: fit based on the expression in the text.

MAR features in Figures 1 and 2. The excess current in a multi-mode junction was theoretically derived in Refs. [?] ADD OTHER REFS. Assuming an equal transparency for the 2 modes in the nanotube, the authors of Ref. [8] obtain the following expression: $I_{ex} = \frac{e\Delta}{h} \frac{G^2}{4-G^2} [1 - \frac{G^2}{4(8-G)\sqrt{4-G}} \ln(\frac{2+\sqrt{4-G}}{2-\sqrt{4-G}})]$ and find an excellent agreement with their data. The result of applying this expression is shown by a dotted line in Figure 6. Clearly, the fit falls short of the experimental data. Most likely the value of Δ is in reality greater than 0.43 meV. Another major source of discrepancy is the assumption of equal transparency of two modes. If one of the modes dominates, in the regime of low transparencies the excess current may be up to two times larger than the above expression.

LONG NANOTUBES

So far, we presented data measured on short nanotube segments, 100 nm in length, where the single-particle energy spacing and level broadening were significantly greater than the superconducting energy gap. The contacts to the nanotubes were rather transparent, so that the Coulomb blockade effect in the nanotubes was suppressed. Therefore, it made sense to characterize the nanotube by an energy-independent transparency that may be controlled by the gate voltage.

We now consider a longer nanotube, with a length of 650 nm, which demonstrates a clear Coulomb blockade pattern. Figure 7a displays the conductance map measured in magnetic field of 0.3 T. The Coulomb blockade “diamonds” are clearly visible, as well as the resonant lines corresponding to the excited states (running parallel to the diamond boundaries) [20]. The extracted Coulomb charging energy (~ 2 meV) and the level spacing (~ 0.5 meV) are comparable to the superconducting gap. Therefore, the nanotube may no longer be considered as a weak link with an energy-independent transmission coefficient. A more involved conductance behavior may be expected as a result of an interplay between several comparable energy scales.

Figure 7b shows the conductance maps measured at zero magnetic field. Clearly, superconductivity in the leads greatly modifies the nanotube conductance. In particular, resonance conductance features appear at $V_{SD} \approx 2\Delta/e$. These features are best visible in the center of the image as lines of constant $V_{SD} \approx \pm 1$ mV. However, in the left and right side of the image, the resonances form a more intricate pattern, where the energies of the conductance resonances depend on the gate voltage. Namely, the resonance positions in V_{SD} curve toward zero at V_{gate} positions corresponding to the single-electron conductance peaks, and grow to approach $\sim 2\Delta/e$ in the Coulomb blockade valleys, in qualitative agreement with the results obtained in multi-wall CNT [6]. Such behavior may be explained by considering Andreev transmission through a resonant weak link [6, 18, 19].

Interestingly, the excited state lines, which in Figure 7a terminate at the boundaries of the Coulomb diamonds, in Figure 7b extend *into* the diamonds. The lines are best visible in Figure 7c, which reproduces the data of Figure 7b with a 5 times greater contrast, in the gate voltage range $-4.9 \text{ V} < V_{gate} < -4.6 \text{ V}$. The resonances approach zero V_{SD} inside the Coulomb diamonds, away from the single-electron conductance peaks. We surmise that these features likely arise due to Multiple Andreev Reflections of quasiparticles transmitted through the resonance levels in the nanotube Quantum Dot.

The appearance of the resonances does not mean that conductance there is enhanced when the leads become superconducting. On the contrary, the conductance inside

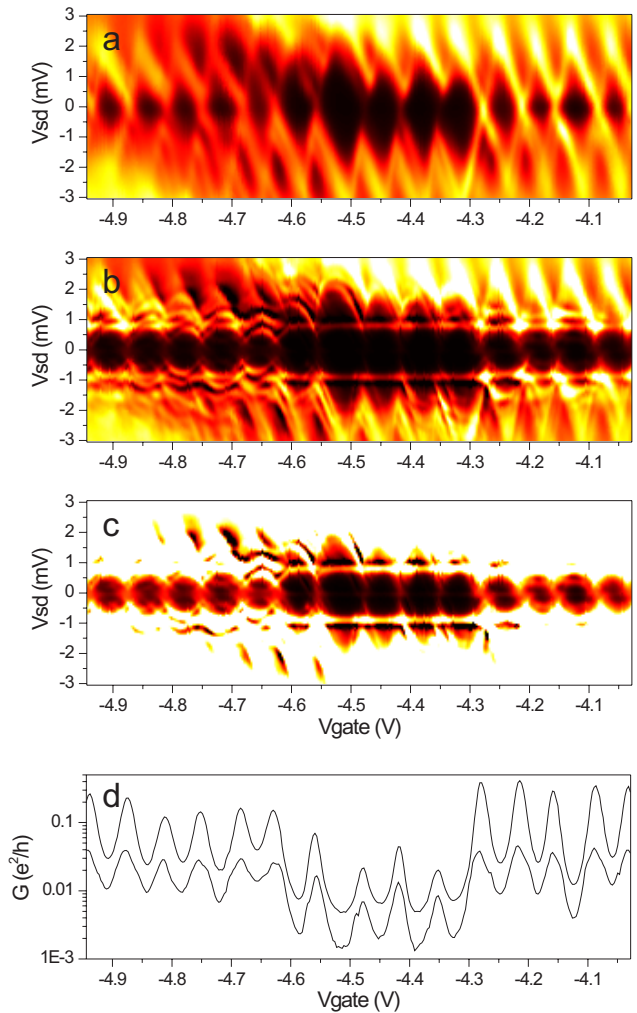


FIG. 7: Differential conductance maps as a function of V_{gate} and V_{SD} at magnetic field of 0.3 T (a) and without magnetic field (b) in case of a well-developed Coulomb blockade in a 650 nm-long nanotube. Colormap: 0 to $0.5 e^2/h$. Establishment of superconductivity in the leads introduces a number of resonant features in b). Same data as in (b) are reproduced in (c) using 5 times greater contrast colormap. d): zero-bias conductance corresponding to Figure 7a (lower curve) and 7b (upper curve). (The curves can be viewed as horizontal cross-sections of Figures 7a,b.) Superconductivity in the leads reduces the zero-bias differential conductance. The suppression is stronger at the single electron peaks (up to tenfold) rather than in the valleys (threefold).

the Coulomb diamonds drops (compare Figures 7a and b). In Figure 7d we plot the zero-bias conductance corresponding to Figures 7a and b (which can be viewed as horizontal cross-sections of these figures). Indeed, in the Coulomb blockade regime, the superconductivity in the leads suppresses the zero-bias differential conductance. Interestingly, the suppression is stronger at the single electron peaks (up to a factor of 10) and weaker in the valleys (about a factor of 3).

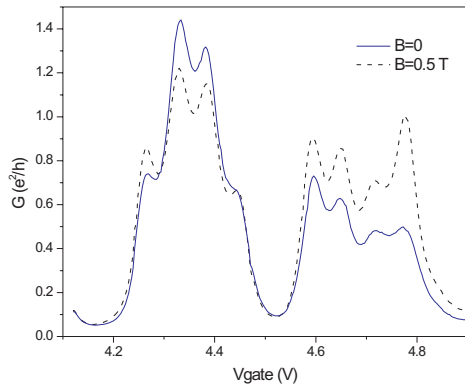


FIG. 8: Differential conductance maps as a function of V_{gate} and V_{SD} at magnetic field of 0.3 T (a) and without magnetic field (b) in case of a well-developed Coulomb blockade in a 650 nm-long nanotube. Colormap: 0 to $0.5 e^2/h$. Establishment of superconductivity in the leads introduces a number of resonant features in b). Same data as in (b) are reproduced in (c) using 5 times greater contrast colormap. d): zero-bias conductance corresponding to Figure 7a (lower curve) and 7b (upper curve). (The curves can be viewed as horizontal cross-sections of Figures 7a,b.) Superconductivity in the leads reduces the zero-bias differential conductance. The suppression is stronger at the single electron peaks (up to tenfold) rather than in the valleys (threefold).

Finally, in Figure 8 we show conductance of another 650 nm - long nanotube with and without magnetic field. This sample clearly shows the

CONCLUSION

In conclusion, we investigate the influence of the superconducting leads on the properties of single-wall carbon nanotubes. For short nanotubes, several transport regimes are observed depending on the normal state transparency. For high transparency, the small-bias conductance grows as the temperature is reduced, and significantly exceeds $4e^2/h$, reaching $10e^2/h$ in some of our samples. We also observe the gap and subgap (Multiple Andreev Reflection) features at lower transparencies. At intermediate transparencies, the temperature dependence of the zero-bias differential conductance may be non-monotonic, where as the temperature decreases the initial rise of dI/dV is replaced by an eventual drop. Finally, in longer nanotubes, where the Coulomb charging energy and the level spacing are comparable to the superconducting gap, we find a complicated pattern of conductance resonances inside the Coulomb diamonds. In this regime, the zero-bias conductance is suppressed stronger at the single-electron conductance peaks rather than in

the valleys.

ACKNOWLEDGEMENTS

We thank D. Averin, D. Bagrets, H. Baranger, A. Golubov, A. Kamenev, A. Levy Yeyati, K. Matveev, and V. Shumeiko for valuable discussions. The work is supported by NSF DMR-0239748.

-
- [1] C. Dekker, *Physics Today*, 22 (1999); P.L. McEuen, *Physics World*, June 2000.
 - [2] A.Y. Kasumov, R. Deblock, M. Kociak, B. Reulet, H. Bouchiat, I.I. Khodos, Y.B. Gorbatov, V.T. Volkov, C. Journet and M. Burghard, *Science* **284**, 1508 (1999).
 - [3] M. Kociak, A.Y. Kasumov, S. Gueron, B. Reulet, I.I. Khodos, Y.B. Gorbatov, V.T. Volkov, L. Vaccarini and H. Bouchiat, *Physical Review Letters* **86**, 2416 (2001).
 - [4] A.F. Morpurgo, J. Kong, C.M. Marcus and H. Dai, *Science* **286**, 263 (1999).
 - [5] M.R. Buitelaar, T. Nussbaumer and C. Schonenberger, *Physical Review Letters* **89**, 256801 (2002).
 - [6] M.R. Buitelaar, W. Belzig, T. Nussbaumer, B. Babic, C. Bruder and C. Schonenberger, *Physical Review Letters* **91**, 057005 (2003).
 - [7] P. Jarillo-Herrero, J.A. van Dam and L.P. Kouwenhoven, *Nature* **439**, 953 (2006).
 - [8] H.I. Jorgensen, K. Grove-Rasmussen, T. Novotny, K. Flensberg and P.E. Lindelof, *Physical Review Letters* **96**, 207003 (2006); K. Grove-Rasmussen, H. I. Jorgensen, and P. E. Lindelof, arXiv:cond-mat/0601371.
 - [9] B. Zheng, C.G. Lu, G. Gu, A. Makarovski, G. Finkelstein and J. Liu, *Nano Letters* **2**, 895 (2002).
 - [10] A.K. Gupta, L. Cretinon, N. Moussy, B. Pannetier and H. Courtois, *Physical Review B* **69**, 104514 (2004).
 - [11] W.J. Liang, M. Bockrath, D. Bozovic, J.H. Hafner, M. Tinkham and H. Park, *Nature* **411**, 665 (2001).
 - [12] T.M. Klapwijk, G.E. Blonder and M. Tinkham, *Physica B and C* **110**, 1657 (1982).
 - [13] E.N. Bratus, V.S. Shumeiko and G. Wendin, *Physical Review Letters* **74**, 2110-2113 (1995).
 - [14] D. Averin and A. Bardas, *Physical Review Letters* **75**, 1831 (1995).
 - [15] J.C. Cuevas, A. Martin-Rodero and A.L. Yeyati, *Physical Review B* **54**, 7366 (1996).
 - [16] E. Vecino, M.R. Buitelaar, A. Martin-Rodero, C. Schonenberger and A.L. Yeyati, *Solid State Communications* **131**, 625 (2004).
 - [17] M. Tinkham, *Introduction to Superconductivity*, Second Edition, McGraw-Hill (1996).
 - [18] A.L. Yeyati, J.C. Cuevas, A. Lopez-Davalos and A. Martin-Rodero, *Physical Review B* **55**, R6137 (1997).
 - [19] G. Johansson, E.N. Bratus, V.S. Shumeiko and G. Wendin, *Physical Review B* **60**, 1382 (1999).
 - [20] L.P. Kouwenhoven, C.M. Marcus, P.L. McEuen, S. Tarucha, R.M. Westervelt, and N.S. Wingreen, in *Mesoscopic Electron Transport*, ed. by L.P. Kouwenhoven, G. Schon, and L.L. Sohn, (Kluwer, 1997), p. 105.